Inorganic Chemistry

ARTICLE

pubs.acs.org/IC

π-Extended and Six-Coordinate Iron(II) Complexes: Structures, Magnetic Properties, and the Electrochemical Synthesis of a Conducting Iron(II) Metallopolymer

Brandon Djukic,[†] Takele Seda,[‡] Serge I. Gorelsky,[§] Alan J. Lough,[∥] and Martin T. Lemaire*[,†]

[†]Department of Chemistry, Brock University, St. Catharines, Ontario L2S 3A1, Canada

[‡]Department of Physics and Astronomy, Western Washington University, Bellingham, Washington 98225, United States

[§]Center for Catalysis Research and Innovation, Department of Chemistry, University of Ottawa, Ottawa, Ontario K1N 6N5, Canada

[∥]Department of Chemistry, University of Toronto, Toronto, Ontario M5S 3H6, Canada

Supporting Information

ABSTRACT: Herein, we describe the preparation of three new bidentate π-extended derivatives of the ligand N-phenyl-2-pyridinalimine (ppi) containing a 3-thienyl (**4**) substituent at position 4 of the aniline ring or 2-thienyl (**6**) or phenyl (**2**) substituents at each of the 2,5 positions of the aniline rings. Three iron(2+) complexes (**7**−**9**) containing these ligands were prepared by combining two equivalents each of **2**, **4**, or **6** with $Fe(NCS)_2$, and the resulting neutral, six-coordinate complexes were fully characterized, including with single crystal X-ray diffraction experiments in the case of complexes **7** and **9**. Variable temperature magnetic susceptibility and Mössbauer experiments confirm the presence of spin-crossover in complexes **7** and **8**, and the unusual solid state variable temperature magnetic properties of complex **9** likely result from crystal packing forces. Electropolymerization of the 2,5-dithienyl-substituted complex (**9**) produces a conducting and electrochromic metallopolymer film (poly-**9**).

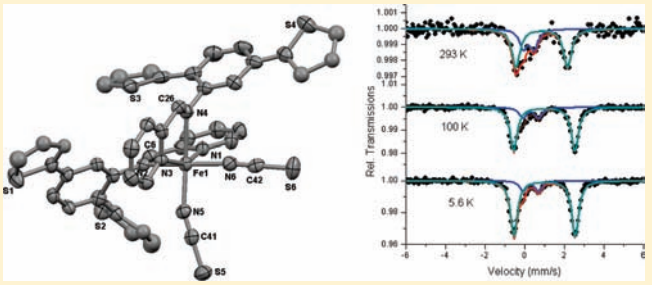

INTRODUCTION

Spin-crossover complexes have been known for over 80 years and are the prototypical examples of molecular switches.[1] In a spin-crossover, there is a reversible thermal-, optical-, or in rare instances pressure-induced change in the spin state of a metal ion (typically Fe^{2+}, Fe^{3+}, or Co^{2+}), and this phenomenon is very well understood from thermodynamic, structural, and magnetic points of view.[2] One recent challenge is to incorporate spin-crossover switching into multifunctional materials to generate new materials with interesting combinations of properties, such as spin-crossover combined with electrical conductivity, liquid crystalline behavior, porosity, or bulk magnetic ordering.[3−6] Our group and others have been interested in the preparation of spin-crossover conductors, which are multifunctional materials exhibiting spin-crossover and electrical charge transport. These unique materials have been prepared either as ionic species featuring cationic iron complexes combined with anionic molecular conductors or as hybrid conducting metallopolymers.[3] In nearly all reported spin-crossover conducting materials, the oxidation state of the iron ion is +3. It is also of interest to prepare spin-crossover conductors featuring iron in the +2 oxidation state for a variety of reasons, including the increased propensity for abrupt spin transitions with thermal hysteresis in iron(2+) complexes as well as the better characterized LIESST properties of iron(2+) as compared with (+3) spin-crossover complexes. Very recently, Oshio and co-workers reported the first example of spin-crossover and electrical conductivity in an iron(2+) complex containing covalently linked tetrathiafulvalene (TTF) substituents.[7]

Previously, we reported the preparation of a conducting poly(terthiophene) metallopolymer containing a covalently linked iron(3+) complex and the observation of spin-crossover and electrical conductivity in this hybrid material.[3d] To produce similar polymers but with iron(2+), we also prepared Toflund-like bispicen ligands containing thiophene-based substituents; nevertheless, under no conditions were we able to electropolymerize the precursor complexes (Figure 1).[8] Another set of ligands which have been used to prepare iron(2+) spin-crossover complexes is based on the neutral bidentate ligand *N*-phenyl-2-pyridinalimine (ppi) and derivatives thereof (Figure 2).[9] For example, the spin-crossover in the complex $Fe(ppi)_2(NCS)_2$ has been extensively studied, and the effect of substitution at the pendant phenyl substituent on the spin-crossover has been investigated by Gütlich and others.[10,11] Of note, substitution with phenylacetylene at the 4 position of the phenyl ring in

Received: May 18, 2011
Published: July 06, 2011

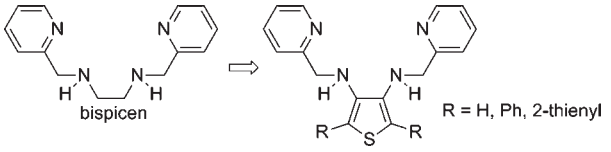

Figure 1. Bispicen ligand of Toflund and structurally analogous derivatives containing substituted thiophenes described in ref 8.

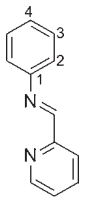

Figure 2. *N*-phenyl-2-pyridinalimine (ppi) ligand used to prepare iron(2+) spin-crossover complexes. Reported derivatives feature two or four substituted anilines.

ppi produces a spin-crossover complex with a wide thermal hysteresis (37 K) centered at room temperature.[12] Herein, we describe the synthesis of three new "π-extended" derivatives of ppi including both phenyl and heteroaryl (2- or 3-thienyl) substituents (at the 4- or 2,5-ring positions of aniline) and the structural, electronic, and variable temperature magnetic and/or Mössbauer properties of six-coordinate and neutral iron(II) complexes containing these ligands. We also describe the electrochemical synthesis of a metallopolymer from one thiophene-bearing complex and the variable temperature magnetic and electrical transport properties of this interesting material.

EXPERIMENTAL SECTION

General Procedures. All reagents were commercially available and used as received unless otherwise stated. Deaerated and anhydrous solvents were obtained from a Puresolve PS MD-4 solvent purification system, and all air- and/or moisture-sensitive reactions were carried out using standard Schlenk techniques. Indium tin oxide (ITO) coated borosilicate glass cuvette slides (5−15 ohms) were purchased from Delta Technologies, Ltd. $^1H/^{13}C$ NMR spectra were recorded on a Bruker Advance 300 MHz spectrometer with a 7.05 T Ultrashield magnet using deuterated solvents. FT-IR spectra were recorded on a Shimadzu IRAffinity spectrometer as thin films deposited by evaporation of CH_2Cl_2 solutions on KBr plates. EI/FAB mass spectra were obtained using a Kratos Concept 1S High Resolution E/B mass spectrometer. UV−vis measurements were recorded on a Shimadzu 3600 UV−vis−NIR spectrophotometer in CH_2Cl_2 solution using quartz cuvette cells. Elemental analyses were carried out by Guelph Chemical Laboratories LTD, Guelph, Ontario, Canada. EDX spectra were obtained on a Pentafet EDS with Link Systems detector (beryllium windows, 20 kV energy).

Electrochemical Measurements. Cyclic voltammetry (CV) and differential pulse voltammetry (DPV) experiments were performed with a Bioanalytical Systems Inc. Epsilon electrochemical workstation. Compounds were dissolved in anhydrous solvent (CH_2Cl_2) and then deareated by sparging with N_2 gas for 20 min. Solution concentrations were approximately 10^{-3} M in **1** containing 0.5 M supporting electrolyte (Bu_4NPF_6). A typical three-electrode setup was used, including a platinum working electrode, Ag wire pseudoreference electrode, and a platinum wire auxiliary electrode. Ferrocene was used in all cases as an internal standard and was oxidized at a potential of +0.51 V in our setup; all potentials quoted are versus the ferrocene oxidation potential. The scan rate for all CV experiments was 100 mV/s. Parameters for the DPV experiments included a pulse amplitude of 50 mV, pulse width of 50 ms, and pulse period of 100 ms; scan rates were 40 mV/s.

Table 1. Crystallographic Data for 7 and 9

compound	7	9
formula	$C_{50.5}H_{37}ClFeN_6S_2$	$C_{49}H_{36}FeN_6S_6$
fw	883.28	957.02
dimensions (mm)	0.60 × 0.20 × 0.08	0.20 × 0.08 × 0.02
a (Å)	17.3899(11)	10.1613(5)
b (Å)	9.6294(6)	15.1701(9)
c (Å)	26.6152(17)	16.5684(10)
cryst syst	monoclinic	triclinic
α (deg)	90	102.549(3)
β (deg)	105.551(3)	91.113(4)
γ (deg)	90	106.291(3)
volume (Å^3)	4293.7(5)	2384.1(2)
space group	$P21/n$	$P\bar{1}$
Z	4	2
μ (mm^{-1})	0.555	0.620
T (K)	150(1)	150(2)
independent reflns	7436, R_{int} = 0.1196	8363, R_{int} = 0.102
number params	564	570
R_1 [$F^2 > 2\sigma(F^2)$]	0.0923	0.0706
wR_2 (F^2)[a]	0.2482	0.1906

[a] $w = 1/[\sigma^2(F_o^2) + (0.069P)^2 + 0.2902P]$ where $P = (F_o^2 + 2F_c^2)/3$.

Spectroelectrochemical Measurements. Spectroelectroelectrochemical experiments were performed using a Bioanalytical Systems Inc. Epsilon electrochemical workstation and a Shimadzu UV-3600 spectrophotometer on poly 1 films deposited on ITO-coated borosilicate glass slides. UV−visible spectra were recorded between 400 and 800 nm at applied potentials of 100, 400, 500, 600, and 900 mV.

X-Ray Structure Determination. A suitable crystal of **4** was mounted on a glass fiber. Data were collected at room temperature (293 K) on a SMART APEX II diffractometer with Mo Kα radiation (λ = 0.71073 Å) located at the McMaster Analytical X-ray Diffraction Facility (MAX). Data were processed using APEX v2.2.0 and solved by direct methods (SHELXS-97). Crystals of **7** and **9** of suitable size were mounted on a glass fiber. Data were collected on a Bruker-Nonius Kappa-CCD diffractometer using monochromated Mo Kα radiation and were measured using a combination of ϕ scans and ω scans with κ offsets, to fill the Ewald sphere. The data were processed using the Denzo-SMN package.[13] Absorption corrections were carried out using SORTAV.[14] The structure was solved and refined using SHELXTL V6.1 for full-matrix least-squares refinement that was based on F^2.[15] All H atoms were included in calculated positions and allowed to refine in riding-motion approximation with U∼iso∼ tied to the carrier atom. In complex **7**, the asymmetric unit contains a half occupancy dichloromethane solvent molecule. The S atom of one of the thiocyanate ligands is disordered over two sites with refined occupancies of 0.61(2) and 0.39(2). For complex **9**, all four thiophene rings are rotationally disordered by approximately 180° with the ratio of the refined occupancies being 0.869(6)/0.131(6), 0.866(6)/0.134(6), 0.810(6)/0.190(6), and 0.643(6)/0.357(6). Table 1 provides crystallographic data for **7** and **9**.

Variable-Temperature Magnetic Susceptibility Measurements. Solid state variable temperature magnetic susceptibility measurements were recorded on a superconducting quantum interference device (SQUID) magnetometer (Quantum Design MPMS) with a 5.5 T magnet (temperature range 1.8−400 K) in an external field of 0.5 T.

dx.doi.org/10.1021/ic2010503 |*Inorg. Chem.* 2011, 50, 7334–7343

Samples of **7**−**9** were carefully weighed into gelatin capsules, which were loaded into plastic straws and attached to the sample transport rod. The magnetization of the samples was scanned over a temperature range of 5−325 K and then back to 5 K (for **7** and **8**), or from 2 to 325 K and then back to 2 K for **9**. Diamagnetic corrections to the paramagnetic susceptibilities were accomplished using Pascal's constants. Variable temperature magnetic susceptibility data from films of poly-**9** were obtained by cutting ITO-coated cuvette slides containing freshly prepared (and vacuum-dried) electrodeposited films of poly-**9** to fit in a plastic straw; the mass of the film was consistently 0.1 mg. Background data were obtained by carefully removing the poly-**9** film from the ITO-coated glass (gently wiping with an ethanol saturated kimwipe) and repeating the SQUID experiment exactly (identical applied field and sequence) on the film free ITO-coated glass. In a typical experiment, a data point was obtained in settle mode (with a 60 s wait for temperature stability before DC scan) every 5 K (between 330 and 120 K) and every 2.5 K between 120 and 5 K. Four scans were obtained for each temperature point.

Mössbauer Spectroscopy. Mössbauer spectra were recorded with a constant-acceleration spectrometer (Wissel GMBH, Germany) in a horizontal transmission mode using a 50 mCi ^{57}Co source. A Janis SHI-850-1 closed cycle helium refrigerator cryostat was used for variable temperature measurements. All spectra were fitted by Lorentzian line shapes using NORMOS (Wissel GMBH) least-squares fitting program. The velocity scale was normalized with respect to metallic iron at room temperature; hence all isomer shifts were recorded relative to metallic iron.

Film Thickness Measurements. The thicknesses of the poly-**9** film and ITO were 130 and 140 nm, respectively, and were measured with a Michelson interferometer using a WILD M8 Stereomicroscope fitted with a LEITZ WETZLAR interferometer lens.

Variable Temperature Resistivity Measurements. The cryostat consisted of a Lakeshore Cryotronics temperature controller (model DRC 91C), CTI-Cryogenics 8001 controller, 8003 compressor, and a CTI-Cryogenics Cryo-Torr 8 high vacuum pump. The temperature dependence of the resistivity data was measured with a standard four probe dc technique and collected on MPMS MultiVu Application software (revision 1.57, build 075). The probes were made by adhering gold wires to the surface of the film with small amounts of silver paint and then soldering the wires to the cryostat sample holder. The film was carefully inspected to ensure that it contained no cracks and that the contact between the film, each gold wire, and the cryostat sample holder remained uninterrupted. The sample holder was fitted into the cryostat sample chamber and then placed under a vacuum. A current of 2.0 mA was applied to the circuit using a Keithly 224 programmable current source, and then the variable temperature resistivity measurements were initiated. For temperature stabilization measurements, the same four probe technique was used, but the data were collected and recorded on a SQUID magnetometer.

Computational Details. All DFT calculations were performed using the Gaussian 03 package using the B3LYP hybrid functional and the TZVP basis set for all atoms.[16] Tight SCF convergence criteria were used for all calculations. The converged wave functions were tested to confirm that they correspond to the ground-state surface. The evaluation of atomic charges and spin densities was performed using the natural population analysis (NPA).[17] The analysis of molecular orbitals in terms of fragment orbital contributions was carried out using the AOMix program.[18] Time-dependent DFT (TD-DFT) calculations at the B3LYP/TZVP level were performed to calculate the absorption spectra as previously described.[19]

Synthesis. *2,5-Diphenylaniline (**1**).* 2,5-Dibromoaniline (0.74 g 3.4 mmol) was added to a round-bottom flask and then combined with anhydrous 1,2-dimethoxyethane (100 mL) and a 1.0 M aqueous solution of K_2CO_3 (30 mL). The mixture was purged by N_2 sparging for 0.5 h, followed by the addition of 2-thienylboronic acid (0.83 g, 6.8 mmol) and $Pd(PPh_3)_4$ (0.39 g, 0.34 mmol). The reaction mixture was heated at 95 °C for 72 h. The reaction contents were combined with H_2O (200 mL) containing 20 g of NaCl and extracted into CH_2Cl_2 (200 mL). The organic extracts were combined, dried over $MgSO_4$, concentrated (not to dryness) by rotary evaporation, dissolved in hexanes, and then filtered through Celite. The filtrate was concentrated to dryness to obtain a white solid. Yield: 480 mg (65%). Mp: 186−187 °C. ^{1}H NMR (300 MHz, $CDCl_3$): δ 7.69 (m, 10H), 7.29 (d, 1H, J = 5.9 Hz), 7.15 (d, 1H, J = 6.3 Hz), 7.05 (s,1H) ppm. ^{13}C NMR (151 MHz, $CDCl_3$): δ 143.9, 141.6, 141.1, 139.3, 130.9, 129.1, 128.9, 128.7, 127.30, 127.28, 127.1, 126.8, 117.7, 114.3 ppm. MS (EI +): m/z 245 [M^+, 100%]. HRMS (EI +) calculated for $[C_{18}H_{15}N]^+$: 245.12045. Found: 245.12008. FT-IR (KBr): 3448 (m), 3374 (m), 3018 (w), 1611 (s), 1555 (m), 1477 (m), 1408 (m), 1311 (w), 1259 (w), 1219 (w), 1148 (w), 1069 (w), 1011 (w), 860 (w), 812 (w), 756 (s), 698 (s) cm^{-1}.

*N-2,5-Diphenyl-N-(pyridin-2-ylmethylidene)aniline (**2**).* Compound **1** (168 mg, 0.69 mmol) was dissolved in 0.5 mL of DCM and added dropwise at room temperature to a solution of pentane containing 2-pyridinecarboxaldehyde (100 mg, 0.93 mmol). The solution was concentrated to 10 mL and cooled. The resulting white precipitate was washed with cool pentane and dried under vacuum conditions. Yield: 191 mg (83%). Mp: 119−121 °C. ^{1}H NMR (300 MHz, $CDCl_3$): δ 8.74 (s, 1H), 8.73 (d, 1H, J = 4.9 Hz), 8.09 (d, 1H, J = 7.9 Hz), 7.80 (m, 3H), 7.64 (m, 12H) ppm. ^{13}C NMR (151 MHz, $CDCl_3$): δ 161.1, 154.9, 149.6, 149.1, 141.5, 140.3, 139.1, 136.7, 134.7, 130.9, 130.3, 128.9, 127.8, 127.7, 127.1, 127.0, 125.4, 125.1, 121.9, 117.4 ppm. MS (EI +): m/z 334 [M^+, 62%], 256 [$(M - C_5H_4N)^+$, 100%)]. HRMS (EI +) calculated for $[C_{24}H_{18}N_2]^+$: 334.14700. Found: 334.14756. FT-IR (KBr): 3055 (m), 2920 (m), 2857 (w), 1629 (m), 1589 (m), 1472 (s), 1438 (m), 1386 (w), 1263 (m), 1182 (w), 1080 (w), 1034 (w), 991 (w), 901 (m), 837 (w), 756 (s), 698 (s) cm^{-1}. Elemental analysis calculated (found) % for $C_{24}H_{18}N_2$: C, 86.20 (85.75); H, 5.43 (5.07); N, 8.38 (8.48).

*4-(Thiophen-3-yl)aniline (**3**).* 4-Iodoaniline (0.219 g 1.00 mmol) was added to a round-bottom flask and then combined with anhydrous 1,2-dimethoxyethane (15 mL) and a 1.0 M aqueous solution of K_2CO_3 (10 mL). The mixture was purged by N_2 sparging for 0.5 h, followed by the addition of 2-thienylboronic acid (0.127 g, 1.00 mmol) and $Pd(PPh_3)_4$ (0.058 g, 0.05 mmol). The reaction mixture was heated at 95 °C for 72 h. The reaction contents were combined with H_2O (200 mL) containing 20 g of NaCl and extracted into CH_2Cl_2 (200 mL). The organic extracts were combined, dried over $MgSO_4$, concentrated (not to dryness) by rotary evaporation, dissolved in hexanes, and then filtered through Celite. The hexanes were then discarded, and the Celite pad containing **3** was washed with $CHCl_3$, concentrated, and then combined with pentane. A red precipitate that appeared instantly was removed by filtration, followed by concentrating the pentane solution to 10 mL and collecting a yellow solid precipitate. Yield: 55 mg (31%). Mp: 96−98 °C. ^{1}H NMR (300 MHz, $CDCl_3$): δ 7.45 (d, 2H, J = 8.5 Hz), 7.41 (m, 3H), 6.67 (d, 2H, J = 8.5 Hz), 3.72 (br, 2H) ppm. ^{13}C NMR (151 MHz, $CDCl_3$): δ 145.6, 142.4, 127.5, 126.7, 126.1, 125.8, 118.0, 115.3 ppm. MS (EI +): m/z 175 [M^+, 100%]. HRMS (EI +) calculated for $[C_{10}H_9NS_1]^+$: 175.04557. Found: 175.04594. FT-IR (KBr): 3406 (br, s), 3314 (m), 3093 (w), 2922 (w), 1618 (s), 1497 (m), 1267 (m), 1196 (m), 1126 (w), 1094 (w), 837 (m), 777 (s), 698 (m), 628 (m), 565 (m), 511 (m) cm^{-1}.

*N-(Pyridin-2-ylmethylidene)-4-(thiophen-3-yl)aniline (**4**).* Compound **3** (50 mg, 0.29 mmol) was dissolved in 1 mL of DCM and added dropwise to a solution of pentane (10 mL) containing 2-pyridinecarboxaldehyde (33.6 mg, 0.31 mmol) at room temperature. The solution was concentrated to 3 mL by slow evaporation. The resulting yellow precipitate was collected by vacuum filtration, washed with cool pentane, and dried. Yield: 63 mg (84%). Mp: 117−120 °C. ^{1}H NMR

(300 MHz, $CDCl_3$): δ 8.76 (d, 1H, J = 4.2 Hz), 8.69 (s, 1H), 8.26 (d, 1H, J = 7.9 Hz), 7.88 (td, 1H, J = 7.6, 1.7 Hz), 7.70 (d, 2H, J = 8.5 Hz), 7.51 (m, 1H), 7.46 (m, 5H) ppm. ^{13}C NMR (151 MHz, $CDCl_3$): δ 160.2, 154.6, 149.8, 141.7, 136.7, 134.5, 127.8, 127.2, 126.3, 126.2, 125.1, 121.9, 121.7, 120.2 ppm. MS (EI +): m/z 264 [M^+, 100%]. HRMS (EI +) calculated for $[C_{16}H_{12}N_2S]^+$: 264.70212. Found: 264.07204. FT-IR (KBr): 3435 (br, m), 3065 (w), 2920 (w), 1622 (br, m), 1472 (m), 1423 (m), 1350 (w), 1261 (m), 1202 (m), 1101 (br, m), 1034 (m), 833 (w), 783 (s), 538 (m) cm^{-1}. Elemental analysis calculated (found) % for $C_{16}H_{12}N_2S$: C, 72.71 (71.94); H, 4.58 (4.72); N, 10.60 (9.89).

*2,5-Bis(thiophen-2-yl)aniline (**5**).* 2,5-Dibromoaniline (0.453 g 2.16 mmol) was added to a round-bottom flask and then combined with anhydrous 1,2-dimethoxyethane (34 mL) and a 1.0 M aqueous solution of K_2CO_3 (17 mL). The mixture was purged by N_2 sparging for 0.5 h, followed by the addition of 2-thienylboronic acid (0.829 g, 6.48 mmol) and $Pd(PPh_3)_4$ (0.250 g, 0.22 mmol). The reaction mixture was heated at 95 °C for 72 h. The reaction contents were combined with H_2O (200 mL) containing 20 g of NaCl and extracted into CH_2Cl_2 (200 mL). The organic extracts were combined, dried over $MgSO_4$, concentrated (not to dryness) by rotary evaporation, dissolved in hexanes, and then filtered through Celite. The filtrate was concentrated to dryness to obtain an orange oil. Yield: 305 mg (55%). ^{1}H NMR (300 MHz, $CDCl_3$): δ 7.42 (m, 3H), 7.34 (dd, 1H, J = 5, 0.5 Hz), 7.30 (dd, 1H, J = 3.5, 0.8 Hz), 7.20 (dd, 1H, J = 3.6, 1.5 Hz), 7.18 (m, 2H), 7.08 (d, 1H, J = 1.6 Hz), 4.12 (br, 2H) ppm. ^{13}C NMR (151 MHz, $CDCl_3$): δ 144.4, 144.2, 140.9, 135.0, 131.5, 128.1, 127.8, 125.9, 125.4, 124.9, 123.3, 119.4, 116.5, 113.2 ppm. MS (EI +): m/z 257 [M^+, 100%]. HRMS (EI +) calculated for $[C_{14}H_{11}NS_2]^+$: 257.03329. Found: 257.03344. FT-IR (KBr): 3443 (br, w), 2924 (s), 2857 (w), 1612 (s), 1552(w), 1483 (m), 1427 (w), 1308 (w), 1260 (w), 1198 (w), 1088 (w), 1049 (w), 949 (w), 839(w), 804 (s), 698 (s), 447 (w) cm^{-1}.

*N-(Pyridin-2-ylmethylidene)-2,5-bis(thiophen-2-yl)aniline (**6**).* Compound **5** (245 mg, 0.95 mmol) was dissolved in 2 mL of DCM and added dropwise to a solution of hexane (4 mL) containing 2-pyridinecarboxaldehyde (150 mg, 1.40 mmol) at room temperature. The resulting yellow precipitate was collected by vacuum filtration, washed with cool pentane, and dried. Yield: 190 mg (58%). Mp: 155−158 °C. ^{1}H NMR (300 MHz, $CDCl_3$): δ 8.78 (d, 1H, J = 4.7), 8.74 (s, 1H), 8.43 (d, 1H, J = 7.8), 7.93 (t, 1H, J = 7.7), 7.83 (d, 1H, J = 8.2), 7.60 (dd, 1H, J = 8.2, 1.6), 7.51 (d, 1H, J = 3.7), 7.46 (m, 4H), 7.34 (d,1H, J = 5.0), 7.14 (m, 2H) ppm. ^{13}C NMR (151 MHz, $CDCl_3$): δ 161.2, 154.6, 149.7, 147.6, 143.4, 140.0, 136.8, 134.3, 128.4, 128.2, 127.6, 127.5, 126.8, 125.9, 125.4, 125.2, 124.2, 123.4, 122.5, 115.9 ppm. MS (EI +): m/z 346 [M^+, 62%], 268 [$(M - C_5H_4N)^+$, 100%]. HRMS (EI +) calculated for $[C_{20}H_{14}N_2S_2]^+$: 346.05984. Found: 346.06023. FT-IR (film, KBr): 3063 (w), 2916 (w), 1620 (m), 1582 (w), 1464 (m), 1431 (m), 1402 (w), 1352 (w), 1211 (w), 1119 (w), 978 (w), 897 (w), 874 (w), 852 (w), 817 (s), 781 (w), 700 (s), 617 (w), 478 (w) cm^{-1}. Calculated for $C_{20}H_{14}N_2S_2$ (found %): C, 69.35 (69.41); H, 4.07 (4.31); N, 8.09 (7.87).

*[Fe(**2**)$_2$(NCS)$_2$] (**7**).* A solution of KSCN (201 mg, 2.06 mmol) in MeOH (50 mL) was sparged with N_2 gas for 0.5 h, combined with $Fe(II)SO_4 \cdot 7H_2O$ (81 mg, 0.29 mmol). The mixture was stirred for an additional 0.5 h and then combined with **2** (191 mg, 0.57 mmol). The solution was stirred under a N_2 atmosphere for 3 days, concentrated to 20 mL, and cooled in an ice bath. The resulting blue precipitate was collected by vacuum filtration and washed with water and pentane and dried. Yield: 210 mg (85%). Crystals suitable for X-ray diffraction were grown by slow evaporation of 50:50 CH_2Cl_2/toluene solutions of **7**. MS (FAB +): m/z 840 [M^+, 3%], 782 [$(M - SCN)^+$, 24%], 448 [$(M - C_{25}H_{18}N_3S)^+$, 100%]. FTIR (KBr): 2963 (m), 2850 (m), 2060 (s), 1591 (br, m), 1471 (m), 1440 (w), 1261 (s), 1098 (s), 1020 (s), 800 (s), 700 (m) cm^{-1}. Elemental analysis calculated (found) % for $C_{50}H_{36}N_5S_2Fe \cdot 0.5CH_2Cl_2$: C, 68.67 (68.93); H, 4.22 (4.68); N, 9.51 (9.34). UV−vis (CH_2Cl_2): λ_{max} (ε(M^{-1} cm^{-1})) 621 nm (1510).

*[Fe(**4**)$_2$(NCS)$_2$] (**8**).* A solution of KSCN (93 mg, 0.96 mmol) in MeOH (50 mL) was sparged with N_2 gas for 0.5 h, combined with $Fe(II)SO_4 \cdot 7H_2O$ (132 mg, 0.47 mmol). The mixture was stirred for an additional 0.5 h and then combined with **4** (250 mg, 0.95 mmol). The solution was stirred under an atmosphere of nitrogen for 3 days, concentrated to 20 mL, and cooled in an ice bath. The resulting green precipitate was collected by vacuum filtration and washed with water and pentane and then dried. Yield: 312 mg (94%). MS (FAB +): m/z 700 [M^+, 10%], 642 [$(M - SCN)^+$, 60%], 378 [$(M - C_{17}H_{12}N_3S_2)^+$, 100%]. FT-IR (KBr): 3092 (w), 2064 (s), 2037 (s), 1589 (br, m), 1487 (w), 1433 (w), 1354 (w), 1300 (w), 1258 (w), 1200 (m), 1150 (w), 1105 (w), 1015 (w), 962 (w), 904 (w), 853 (w), 785 (m), 731 (w), 689 (w), 629 (w), 554 (w) cm^{-1}. Elemental analysis calculated (found)% for $C_{34}H_{24}N_6S_5Fe$: C, 58.29 (58.31); H, 3.45 (3.12); N, 12.00 (11.92). UV−vis (CH_2Cl_2): λ_{max} (ε (M^{-1} cm^{-1})) 630 nm (1690).

*[Fe(**6**)$_2$(NCS)$_2$] (**9**).* A solution of KSCN (73 mg, 0.75 mmol) in H_2O (10 mL) was sparged with N_2 gas for 0.5 h and then combined with $Fe(II)SO_4 \cdot 7H_2O$ (69 mg, 0.25 mmol). The mixture was stirred for an additional 0.5 h and then combined with a solution of **6** (170 mg, 0.50 mmol) in MeOH (50 mL), which was also sparged with N_2 gas for 0.5 h. The solution was stirred under a N_2 atmosphere for 72 h, concentrated to 20 mL, and cooled in an ice bath. The resulting green-blue precipitate was collected by vacuum filtration and washed with water and pentane and then dried. Yield: 220 mg (65%). Crystals suitable for X-ray diffraction were grown by slow evaporation of 50:50 CH_2Cl_2/toluene solutions of **9**. MS (FAB +): m/z 864 [$(M)^+$, 3%], 806 [$(M - SCN)^+$, 27%], 460 [$(M - C_{21}H_{14}N_3S_3)^+$, 100%]. FT-IR (KBr): 3066 (w), 2924 (w), 2852 (w), 2054 (s), 1625 (br, m), 1593 (s), 1483 (m), 1439 (m), 1301 (w), 1211 (w), 1120 (w), 955 (w), 910 (w), 817 (m), 773 (w), 698 (s) cm^{-1}. Recrystallized powder, calculated for $C_{56}H_{44}N_6S_6Fe \cdot CH_2Cl_2$ (found %): C, 60.37 (60.41); H, 4.09 (3.46); N, 7.42 (7.48). Precipitated powder, calculated for $C_{42}H_{28}N_6S_6Fe$ (found %): C, 58.34 (58.78); H, 3.27 (3.28); N, 9.73 (9.09). UV−vis (CH_2Cl_2): λ_{max} (ε (M^{-1} cm^{-1})) 560 nm (1510).

*poly-**9**.* Prior to electropolymerization, **9** was dried under vacuum conditions at room temperature for 72 h. Complex **9** (0.004 g, 4.63 μmol) was dissolved in anhydrous CH_2Cl_2 (2 mL) containing 0.5 M supporting electrolyte (Bu_4NPF_6) and sparged with N_2 gas for 20 min. The solution was then subjected to successive oxidative sweeps at a scan rate of 100 mV/S over a potential range of −0.5 to +1.0 V (vs ferrocene). An orange film was deposited on the surface of the ITO (or platnium) electrode. FT-IR (KBr pellet): 3449 (br, s), 2961 (w), 2924 (w), 2855 (w), 2667 (m), 1630 (br, s), 1464 (w), 1400 (w), 1261 (w), 1099 (br, w), 1024 (br, w), 845 (br, m), 804 (w), 673 (w), 559 (w) cm^{-1}. UV−vis (ITO): λ_{max} 410 nm.

Scheme 1. Preparation of Ligand 4[a]

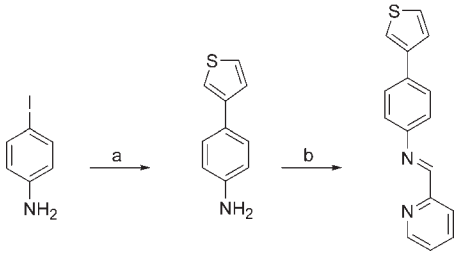

[a] Reagents and conditions: (a) 3-thiopheneboronic acid, DME, H_2O, 5 mol % $Pd(PPh_3)_4$, K_2CO_3, 95 °C, 72 h. (b) 2-pyridinecarboxaldehyde, CH_2Cl_2, pentane.

dx.doi.org/10.1021/ic2010503 |Inorg. Chem. 2011, 50, 7334–7343

RESULTS AND DISCUSSION

Ligand Synthesis, Coordination Chemistry, and Structural Studies. Monothienyl-substituted ligand **4** is prepared in two steps from commercially available 4-iodoaniline. Suzuki–Miyaura cross-coupling produced 4-(3′-thienyl)aniline, which readily undergoes a condensation reaction with 2-pyridinecarboxaldehyde to produce the bidentate ligand (Scheme 1). 2,5-Diaryl substituted ligands [R = phenyl (**2**) or 2-thienyl (**6**)] were prepared similarly, starting from commercially available 2,5-dibromoaniline (Scheme 2). All ligands are analytically pure and were fully characterized. Single crystals were obtained

Scheme 2. Preparation of Ligands 2 and 6[a]

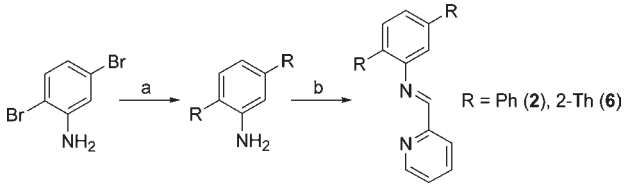

[a] Reagents and conditions: (a) **2**, 2-phenylboronic acid; **6**, 2-thiopheneboronic acid; DME; H_2O; 10 mol % $Pd(PPh_3)_4$; K_2CO_3; 95 °C,; 72 h. (b) 2-pyridinecarboxaldehyde, CH_2Cl_2, pentane.

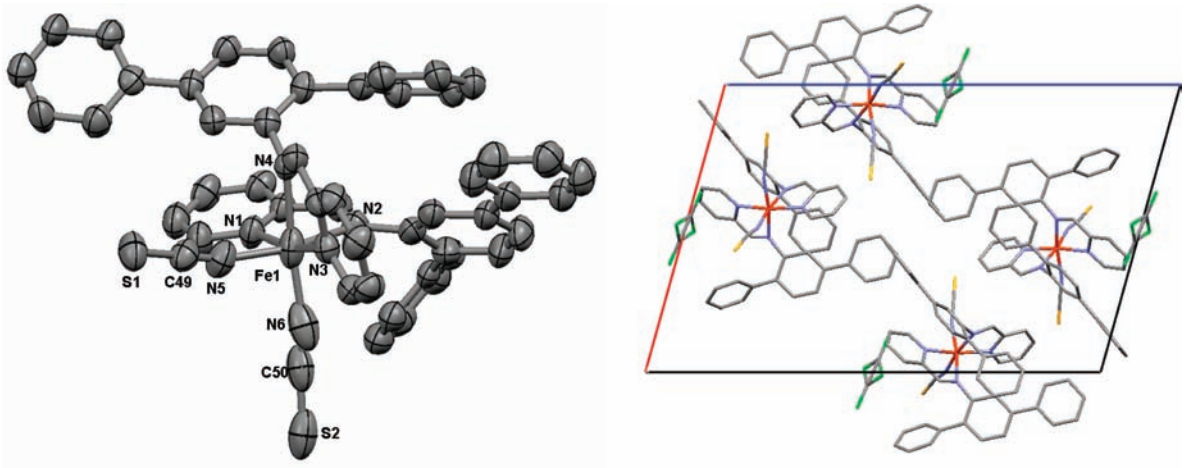

Figure 3. Left: ORTEP diagram of the molecular structure of **7** with thermal ellipsoids drawn at the 50% probability level. H atoms and the disordered CH_2Cl_2 solvate molecule are omitted for clarity. Selected bond distances (Å) and angles (deg): Fe(1)–N(1), 2.052(6); Fe(1)–N(2), 2.097(5); Fe(1)–N(3), 2.069(6); Fe(1)–N(4), 2.119(5); Fe(1)–N(5), 2.023(7); Fe(1)–N(6), 1.99(1); N(1)–Fe(1)–N(2), 78.1(2); N(1)–Fe(1)–N(4), 91.7(2); N(1)–Fe(1)–N(5), 90.6(3); N(1)–Fe(1)–N(6), 96.6(3); N(2)–Fe(1)–N(3), 103.2(2); N(2)–Fe(1)–N(4), 88.5(2); N(2)–Fe(1)–N(6), 92.1(3); N(3)–Fe(1)–N(4), 76.6(2); N(3)–Fe(1)–N(5), 86.8(3); N(3)–Fe(1)–N(6), 95.0(3); N(4)–Fe(1)–N(5), 86.8(3); N(5)–Fe(1)–N(6), 94.3(3); N(1)–Fe(1)–N(3), 168.2(2); N(2)–Fe(1)–N(5), 167.6(3); N(4)–Fe(1)–N(6), 171.5(3). Right: Molecular packing of **7** viewed down the crystallographic *b* axis (disordered CH_2Cl_2 solvent included).

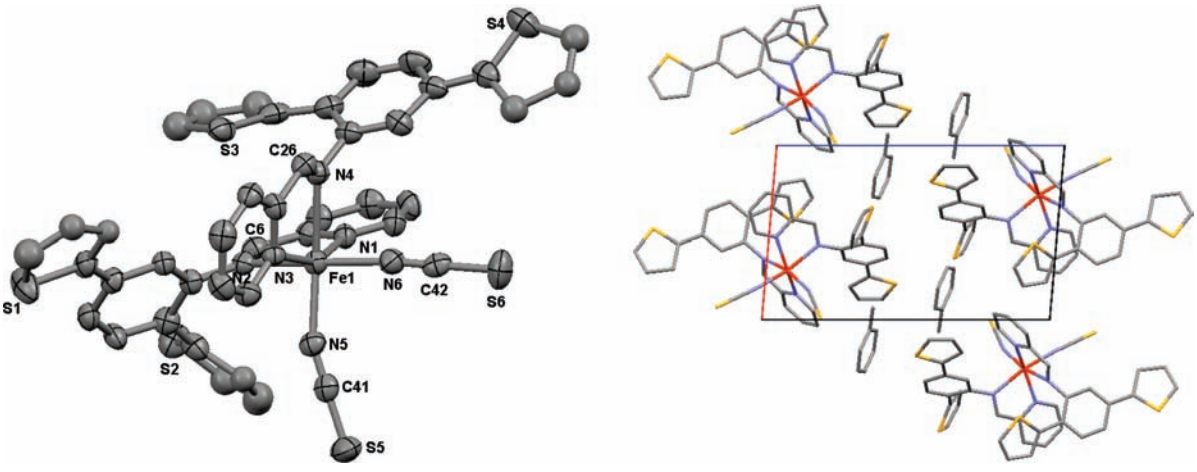

Figure 4. Left: ORTEP diagram of the molecular structure of **9** with thermal ellipsoids drawn at the 50% probability level. H atoms and toluene solvate molecule are omitted for clarity. Selected bond distances (Å) and angles (deg): Fe(1)–N(1), 2.188(3); Fe(1)–N(2), 2.266(4); Fe(1)–N(3), 2.186(4); Fe(1)–N(4), 2.310(5); Fe(1)–N(5), 2.063(5); Fe(1)–N(6), 2.080(5) and N(1)–Fe(1)–N(2), 74.9(1); N(1)–Fe(1)–N(4), 86.1(1); N(1)–Fe(1)–N(5), 109.4(2); N(1)–Fe(1)–N(6), 92.0(2); N(2)–Fe(1)–N(3), 97.2(1); N(2)–Fe(1)–N(4), 100.0(1); N(2)–Fe(1)–N(5), 88.4(2); N(3)–Fe(1)–N(4), 73.0(1); N(3)–Fe(1)–N(5), 92.5(2); N(3)–Fe(1)–N(6), 96.5(2); N(4)–Fe(1)–N(5), 82.9(2); N(5)–Fe(1)–N-(6), 92.1(2); N(1)–Fe(1)–N(3), 156.2(2); N(2)–Fe(1)–N(6), 166.3(2); N(4)–Fe(1)–N(5), 164.0(2). Right: Molecular packing of **9** viewed down the crystallographic *b* axis (toluene solvent included).

dx.doi.org/10.1021/ic2010503 |*Inorg. Chem.* 2011, 50, 7334–7343

from a solution of **6**, and an X-ray diffraction experiment was performed. An ORTEP diagram of the molecular structure of **6** and relevant bond parameters can be found in the Supporting Information (Figure S1).

Iron(II) complexes were prepared under anaerobic conditions by combining two equivalents of ligands **2**, **4**, or **6** with $Fe(NCS)_2$, which was prepared in situ from KSCN and $FeSO_4 \cdot 7H_2O$, to produce complexes **7**−**9** as blue precipitates. Slow evaporation of 1:1 dichloromethane/toluene solutions of **7** and **9** produced crystals of each complex suitable for X-ray diffraction experiments. The molecular structures of **7** and **9** are indicated as ORTEP diagrams in Figures 3 and 4, respectively. Complex **7** crystallized as a dichloromethane solvate and **9** as a toluene solvate with the iron(2+) ion coordinated in the anticipated *cis*-pseudooctahedral geometry in both complexes. Coordinate bond distances are shortest to the *N*-bound thiocyanate, slightly longer to the terminal pyridine rings, longest to the imine N atoms for each complex, and within the range typically encountered with low-spin iron(2+) for **7** and high-spin iron(2+) for **9**. We note that the temperature of the X-ray diffraction experiment (150 K) is nearly at the midpoint of the spin-transition featured for complex **7** (*vida infra*), and so the coordinate bond distances reported likely represent an average for the high and low spin isomers. Our attempts to obtain the X-ray structures at higher temperatures were unsuccessful because of the large amount of structural disorder. One of the coordinated thiocyanate ligands is disordered over two positions in **7**, and all four thiophene rings in **9** are rotationally disordered by approximately 180° over two sites.

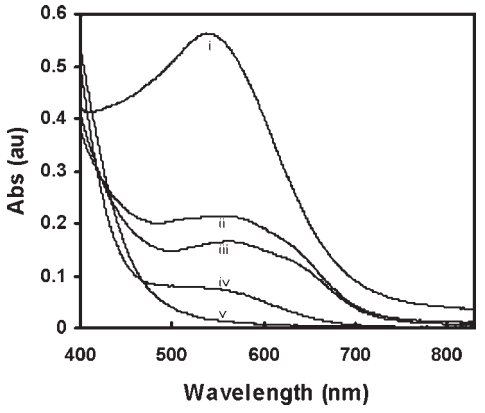

Figure 5. Room temperature UV−vis spectra of **9** in (i) toluene, (ii) CH_2Cl_2, (iii) $CHCl_3$, (iv) CH_3CN, and (v) MeOH.

Table 2. Selected Electrochemical Data[a]

compound	E'_{ox} (V)	E'_{red} (V)
$Fe(ppi)_2(NCS)_2$	0.0, +0.6, +0.9	
4	+0.6, +1.2, +1.5	−1.0, −1.6, −2.2
6	+0.6, +0.7, +1.2	−0.9, −1.5, −2.1
7	0,0, +0.5, +1.3	−1.0, −1.4
8	0.0, +0.6, +1.2	−0.8, −1.6
9	−0.2, +0.4, +0.8, +1.0	−0.8, −1.6

[a] All experiments were performed in CH_2Cl_2, containing 0.5 M $^nBu_4NPF_6$ supporting electrolyte, and all potentials are quoted versus a ferrocene/ferrocenium reference.

Electronic Properties. The electronic properties of compounds **4** and **6**−**9** have been investigated using a combination of UV−visible spectroscopy and/or cyclic (CV) and differential pulse (DPV) voltammetries. The visible spectra for complexes **7**−**9** are typical for 6-coordinate iron(II) complexes with N-donor ligands and feature broad solvatochromic MLCT bands centered at approximately 560 nm (complex **9**, Figure 5).

The electrochemical properties of **4** and **6**−**9** were probed with CV and DPV, and as examples, the voltammograms of **6** (left) and **9** (right) are featured in Figure 6. Important electrochemical data for all compounds are summarized in Table 2. All potentials quoted are referenced to the ferrocene/ferrocenium couple. CVs of $Fe(ppi)_2(NSC)_2$, **4**, **7**, and **8** can be found in the Supporting Information (Figures S2−S5). Thienyl-substituted ligands, **4** and **6**, feature a series of broad and irreversible oxidative processes between +0.6 and 1.5 V, which includes the oxidation of the thiophene heterocycles at the higher potentials. Cathodic scans are unremarkable and contain broad and irreversible features at very negative potentials. For comparison, the CV of $Fe(ppi)_2(NCS)_2$ was measured and the reversible oxidation of

Scheme 3. Electropolymerization of 9 to Produce poly-9[a]

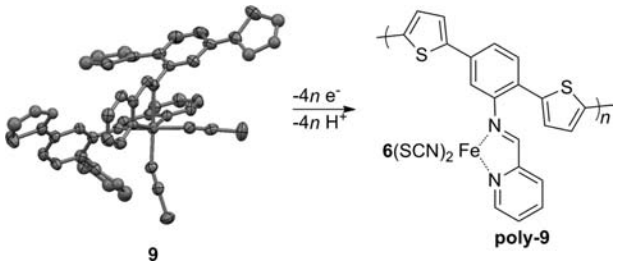

[a] For clarity, only one equivalent of coordinated and polymerized ligand **6** is shown in full in the representation of poly-**9**.

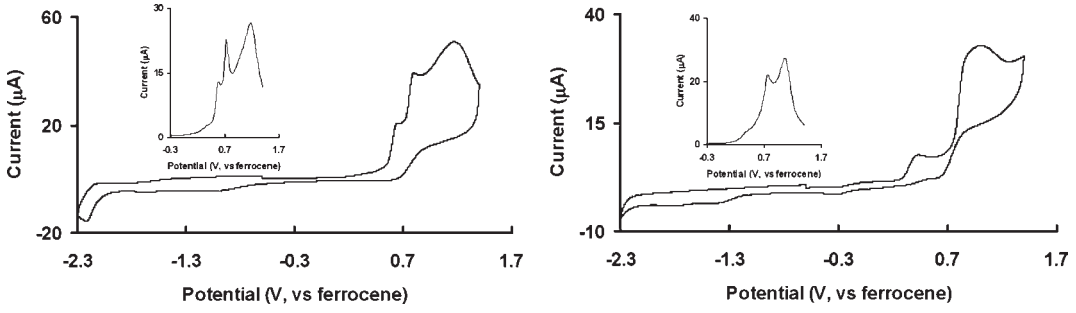

Figure 6. Cyclic voltammograms of 10^{-3} M solutions of **6** (left) and **9** (right) in CH_2Cl_2 containing 0.5 M Bu_4NPF_6 with a scan rate of 100 mV/s. Insets: Differential pulse voltammograms of **6** (left) and **9** (right) obtained with the same parameters as the CV.

dx.doi.org/10.1021/ic2010503 |*Inorg. Chem.* 2011, 50, 7334–7343

the metal occurs at the same potential as ferrocene (0.0 V). Other irreversible features are noted at higher potentials and include oxidation of the thiocyanate ligand (+0.6 V). The CVs of complexes **7**−**9** are dominated by irreversible ligand-centered anodic processes, but weak metal oxidations were noted at potentials similar to that observed in $Fe(ppi)_2(NCS)_2$.

Electropolymerization. Complex **9** was successfully electropolymerized in CH_2Cl_2 solution by repeated voltammetric cycling between a potential window of −0.5 and +1.3 V (vs ferrocene, Figure 7). A linear relationship between the peak current with the number of scans was observed, and the reaction results in the deposition of a brilliant orange film (poly-**9**) on the working electrode (platinum button or indium−tin-oxide-coated borosilicate glass). The current dependence on the scan rate for the washed film in a monomer free CH_2Cl_2 solution is linear, indicating the deposition of an electroactive film (Figure S6 in the Supporting Information). Differential pulse voltammetry experiments on complex **9** and poly-**9** samples indicate that the +2 oxidation state of the metal center is maintained in the polymer film (Figures S7 and S8 in the Supporting Information). The elemental composition of the poly-**9** film was investigated using quantitative energy dispersive X-ray spectroscopy (EDX). The measured Fe/S ratio in the poly-**9** film (0.18) was close to the theoretical value (0.17) and to

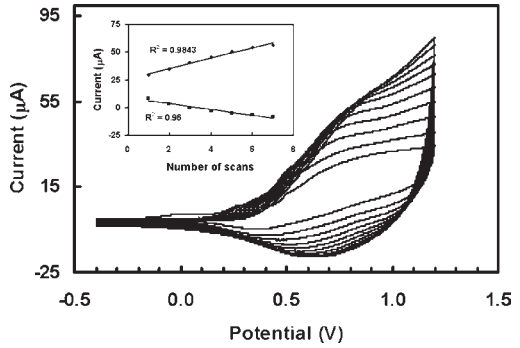

Figure 7. Electropolymerization of **9** in CH_2Cl_2 (inset: plot of linear current increases versus scan number). Potentials are referenced to the ferrocene redox couple.

Table 3. Mössbauer Properties of 8 and 9

compound	T (K)	IS (mm/s)	QS (mm/s)	Fe site (%)	Fe spin state
9	293	0.97(1)	2.60(2)	68	2
		0.32(3)	0.54(5)	32	0
	100	1.103(3)	3.087(7)	80	2
		0.418(8)	0.78(2)	20	0
	5.6	1.107(2)	3.088(5)	85	2
		0.42(1)	0.79(3)	15	0
8	293	0.983(2)	2.731(3)	83	2
		0.29(2)	0.32(2)	17	0
	100	1.25(4)	2.8(1)	7	2
		0.416(2)	0.807(3)	93	0
	5.6	0.421(1)	0.815(2)	>98	0

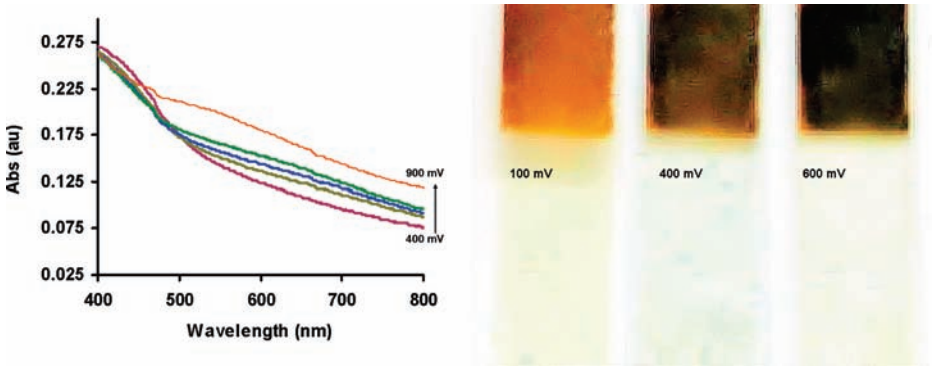

Figure 8. Left: Spectroelectrochemical data for poly-**9**. Right: Electrochromic properties of poly-**9** films deposited on ITO-coated glass slides at applied potentials noted in the figure.

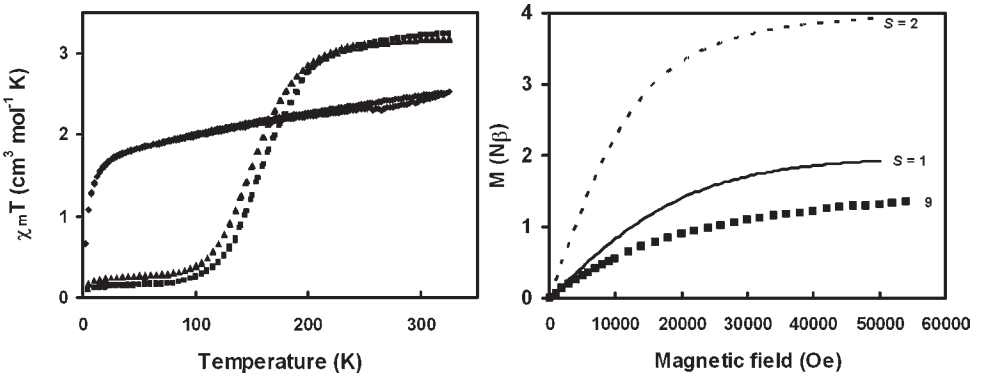

Figure 9. Left: Temperature dependence of $\chi_m T$ values for **7** (▲), **8** (■), and **9** (♦) (5000 Oe field). Right: Reduced magnetization versus field data measured at 2 K. Experimental results for **9** are indicated as squares. Theoretical curves for $S = 2$ and $S = 1$ states are depicted as dashed or solid lines, respectively.

dx.doi.org/10.1021/ic2010503 |*Inorg. Chem.* 2011, 50, 7334–7343

the ratio measured for the complex 1 (0.17, see Supporting Information). All of the spectroscopic data obtained point to the structure of poly-**9** as indicated in Scheme 3.

The visible absorption spectrum of a poly-**9** film deposited on ITO-coated glass features an absorption centered at 410 nm with a broad shoulder at lower energy that spans the visible region (Figure 8, left). The lower energy absorption is attributed to intergap transitions due to residual oxidative doping from the electropolymerization reaction. As noted, the deposited poly-**9** film is a brilliant orange color, and electrochromic properties of poly-**9** are displayed in Figure 8 (right). The film darkens at higher potentials as the metallopolymer is oxidatively doped. Up to approximately 600 mV, the electrochemical oxidation is completely reversible, and poly-**9** can be switched back to its original orange state.

Variable Temperature Magnetic Susceptibility, Mössbauer Spectroscopy, and DFT Calculations. The solid-state temperature dependent magnetic properties of neutral complexes **7**−**9** were investigated using SQUID magnetometry. The temperature dependent profiles are nearly identical for **7** and **8** and feature gradual transitions from high ($\chi_m T$ = 3.2 cm^3 mol K^{-1} at 300 K) to low spin ($\chi_m T$ = 0.1 cm^3 mol K^{-1} at 5 K) centered at approximately 150 K. SQUID measurements were carefully recorded in settle mode, with a 60 s wait prior to DC scan, and there is no evidence of thermal hysteresis upon warming. Variable temperature Mössbauer spectroscopy data (Table 3) obtained from solid samples of **8** essentially mirror the magnetometry results, with essentially complete conversion to low spin iron(2+) noted at 5.8 K (Figure S9 in the Supporting Information).

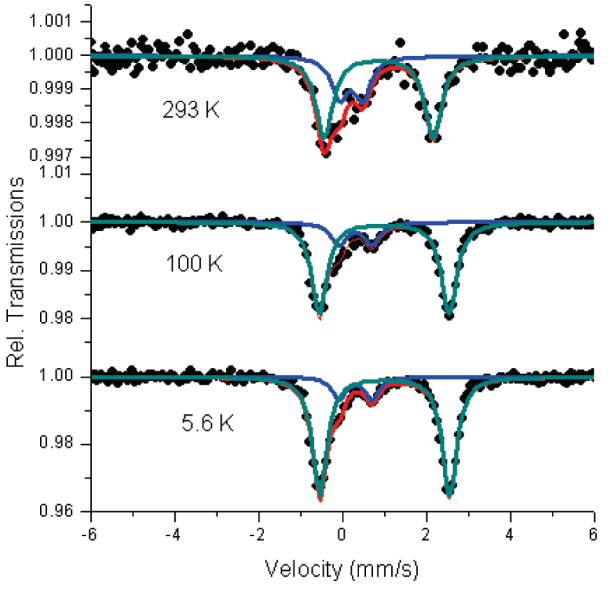

Figure 10. Mössbauer spectra recorded for solid samples of **9** at temperatures indicated in the figure. The dots represent the observed spectra; lines indicate simulated high-spin (green), low-spin (blue), and the sum of high- and low-spin (red) curves.

The variable temperature magnetic properties of **9** are rather different from those of **7** and **8** (Figure 9). For example, the 300 K value of $\chi_m T$ is much less for **9** (2.4 cm^3 K mol^{-1}), and there is no discernible spin- crossover as is readily evident from samples of **7** or **8**, nor are there any obvious intermolecular exchange pathways evident from the X-ray structure. Instead, there is a very gradual decrease in $\chi_m T$ (at 12 K $\chi_m T$ is 1.5 cm^3 K mol^{-1}), the rate of which becomes much faster below 10 K. At 2 K, the $\chi_m T$ value (0.72 cm^3 K mol^{-1}) is significantly higher than the values observed for **7** or **8**. The odd data profile and specific $\chi_m T$ values at low temperatures led us to initially suspect the presence of a stable thermally populated triplet state for **9**. We measured the magnetization of **9** versus the field at 2 K, and the reduced magnetization values do not saturate at 5.5 T but approach a value of 1.3 Nβ, which is less than the theoretical value of 2 anticipated for a pure S = 1 state (Figure 9, right). In CH_2Cl_2 solution, Evans method experiments indicate high-spin iron(2+) over the temperature range 187−295 K with magnetic moments around 5 μ_B.[20] Mössbauer data and computational results (*vida infra*) rule out the possibility of a triplet ground state for **9**.

Mössbauer spectra were recorded on solid samples of **9** at 293, 100, and 5.6 K, which are very different from the spectra obtained from **8** (Figure 10). The quadrupole splitting and isomer shift values (Table 3) indicate high (S = 2) and low (S = 0) spin states in thermal equilibrium with each other, as observed for **8**; however, the proportion of high-spin iron actually increases a little with decreasing temperature, from 68% at 293 K to 85% at 5.6 K. It should be noted, however, that the 293 K Mössbauer spectrum is rather noisy, and the quoted simulated site

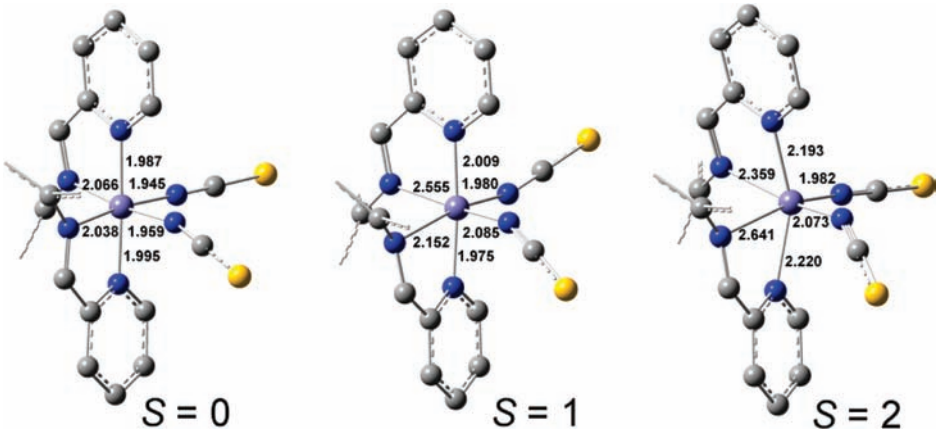

Figure 11. DFT optimized gas phase structures of complex **9** in S = 2 (right), 1 (center), and 0 (left) states with coordinate bond distances (Å) included [in all structures, the 2,5-bis(thiophen-2-yl) substituent is not shown for clarity].

dx.doi.org/10.1021/ic2010503 |*Inorg. Chem.* 2011, 50, 7334–7343

percentages have larger error bars. Below 20 K, the $\chi_m T$ values are observed to decrease somewhat with decreasing temperature, which is likely the result of a combination of zero-field splitting of the $S = 2$ state and weak intermolecular antiferromagnetic interactions.

To shed light on the unusual magnetic properties of complex **9**, density functional theory (DFT) calculations at the B3LYP/TZVP level were used to calculate the gas phase structures and relative energies of complex **9** in a variety of spin states [$S = 2$ (quintet), 1 (triplet), or 0 (singlet)]. DFT-optimized structures of **9** (including calculated coordinate bond lengths) are indicated in Figure 11 for $S = 0$, 1, or 2 spin states. At the temperature of the X-ray diffraction experiment (150 K), there is a substantial population of the $S = 2$ isomer, and the experimental coordinate bond distances agree well with the calculated values (generally within at least ±0.09 Å) in all cases with one exception—the coordinate bond to the imine N atom of one coordinated **6** is calculated to be 2.641 Å, which is significantly greater than the experimental value (2.310(5) Å). Closer inspection of the X-ray structure of **9** indicates an intramolecular short contact between S3 of a thiophene ring and imine N4 within one of the coordinated equivalents of ligand **6** (Figure 12). Crystal packing effects are likely responsible for this interaction since it is not observed in the calculated gas phase structure, and perhaps this interaction is in part influencing the magnetic properties of this complex by presenting a barrier to the coordinate bond length changes that accompany a typical high to low spin-crossover and in fact is actually helping to stabilize the $S = 0$ state at higher temperatures, which is suggested by the Mössbauer data. The calculated electronic energy difference [$\Delta E_{el} = E_{el}(HS) - E_{el}(LS)$] between the quintet and singlet states of **9** is −7.1 kJ/mol, which correctly predicts the quintet state to lie lower in energy than the singlet state. However, it is well-known that the results of these calculations are rather dependent on the choice of functional and for small energy separations, the calculated ground state multiplicity is often incorrect.[21] On the other hand, the triplet state energy is 46.4 kJ/mol higher than the quintet state and is therefore not a factor in the magnetic properties of complex **9**, as we originally supposed. For comparison, the singlet-quintet energy gap in $Fe(ppi)_2(NCS)_2$ was calculated to be 0.4 kJ/mol with the singlet as the ground state.

The temperature dependent magnetic properties of the poly-**9** film were also measured (Figure 13). The diamagnetic contribution of the ITO-coated glass was obtained by measuring the magnetization of the glass after removal of the poly-**9** film. The resulting data are noisy, and repeated attempts to produce better quality data were not successful. We attribute this noise in part to the very small mass of the deposited films. The magnetic moment per repeat unit of poly-**9** at 325 K is approximately 4 μ_B, which is a little lower than the anticipated value of 4.9 μ_B for a single high spin iron(2+) ion, and as the sample is cooled, the magnetic moment steadily decreases. At the lowest measured temperature (5 K), a magnetic moment of 1 μ_B is observed. The residual magnetic moment may be the result of an incomplete spin crossover, a paramagnetic impurity, and/or the magnetic moment contributed by the itinerant electrons in the conducting polymer chain. In addition, a discrepancy in the measured magnetic moment values between warming and cooling, which spans the entire range of measured temperature points (5 − 330 K), was also noted but is very likely the result of measurement errors rather than a real thermal hysteresis. The electrical transport properties of a poly-**9** film deposited on ITO-coated glass were measured using the typical four contact method. Resistivity measurements were conducted by either sweeping the desired temperature range with the sample contained within a liquid helium cooled cryostat (Figure 13) or with the sample inserted into a SQUID magnetometer, which allowed for settling on the desired temperature prior to measurement of the voltage (Figure 13). The results obtained through temperature sweeping

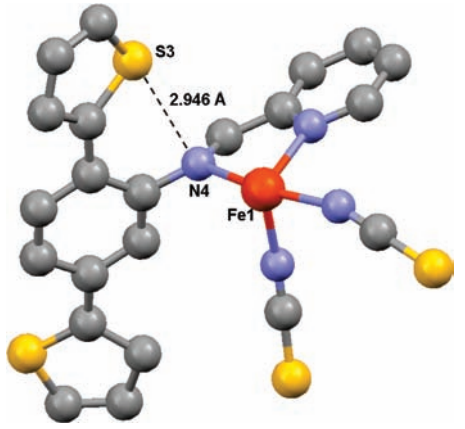

Figure 12. Ball-and-stick representation of the molecular structure of **9**, indicating an intramolecular short contact between S3 and N4 (dotted line). Only one equivalent of coordinated **6** is shown for clarity.

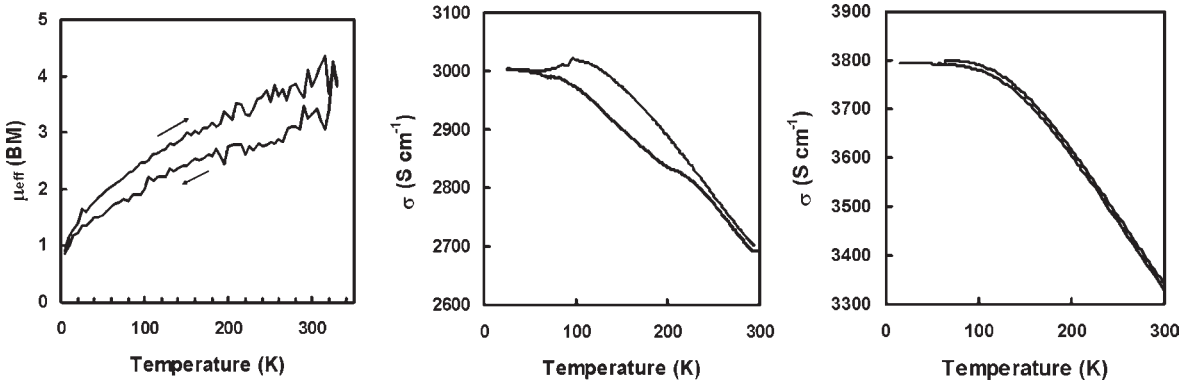

Figure 13. Left: Temperature dependence of $\chi_m T$ values for poly-**9** (15000 Oe field). Center: Variable temperature conductivity profile of poly-**9** measured by sweeping the desired temperature range. Right: Variable temperature conductivity profile of poly-**9** measured by settling on each temperature point.

dx.doi.org/10.1021/ic2010503 |*Inorg. Chem.* 2011, 50, 7334–7343

are very similar to those obtained from a poly(terthienyl) substituted iron(3+) conducting metallopolymer reported earlier and include the same unusual temperature dependent profile.[3d] We also measured the temperature dependence of poly-**9** resistivity using the same four contact technique with the sample located within a SQUID magnetometer (in zero magnetic field), which enabled us to settle and rest on each temperature point prior to making a measurement. In this manner, the resistivity gap between warming and cooling is nearly completely narrowed; however, a small difference in resistivity was observed. This result indicates that the conductivity changes in the poly-**9** film are time dependent and perhaps result from structural changes that accompany the change in spin state or other structural changes in the polymer that are temperature dependent.

CONCLUSIONS

We have described the synthesis of three new ppi-type ligands featuring phenyl and thiophene substituents. Iron(II) complexes containing these ligands were observed to exhibit spin-crossover (complexes **7** and **8**), and unusual behavior was observed in a 2,5-dithienyl substituted complex **9**, which we attribute to crystal packing forces. Incorporating spin-crossover into multifunctional materials is a very active research area, and included in these efforts is the production of spin-crossover conductors for which there is only one reported example containing iron in the +2 oxidation state. Our results suggest that it is possible to electrochemically create hybrid conducting metallopolymers containing iron(II), and spin-crossover may be achieved given the right structural conditions. Current efforts in this regard will be published in due course.

ASSOCIATED CONTENT

Supporting Information. General spectroscopic data and crystallographic data in CIF format. This material is available free of charge via the Internet at http://pubs.acs.org.

AUTHOR INFORMATION

Corresponding Author
*E-mail: mlemaire@brocku.ca.

ACKNOWLEDGMENT

M.T.L. thanks NSERC (Discovery & RTI) and CFI (Leaders Opportunity Fund) for financial support.

REFERENCES

(1) Cambi, L.; Szego, L. *Chem. Ber. Dtsch. Ges.* **1931**, *64*, 2591.
(2) (a) Gamez, P.; Costa, J. S.; Quesada, M.; Aromi, G. *Dalton Trans.* **2009**, 7845. (b) Murray, K. S. *Eur. J. Inorg. Chem.* **2008**, 3101. (c) Halcrow, M. A. *Polyhedron* **2007**, *26*, 3523. (d) Nihei, M.; Shiga, T.; Maeda, Y.; Oshio, H. *Coord. Chem. Rev.* **2007**, *251*, 2606.
(3) (a) Takahashi, K.; Cui, H.-B.; Okano, Y; Kobayashi, H.; Einaga, Y.; Sato, O. *Inorg. Chem.* **2006**, *45*, 5739. (b) Faulmann, C.; Jacob, K.; Dorbes, S.; Lampert, S.; Malfant, I.; Doublet, M.-L.; Real, J. A. *Inorg. Chem.* **2007**, *46*, 8548. (c) Takahashi, K.; Cui, H.-B.; Okano, Y.; Kobayashi, H.; Mori, H.; Tajima, H.; Einaga, Y.; Sato, O. *J. Am. Chem. Soc.* **2008**, *130*, 6688. (d) Djukic, B; Lemaire, M. T. *Inorg. Chem.* **2009**, *48*, 10489.
(4) (a) Seredyuk, M.; Gaspar, A. B.; Ksenofontov, V.; Galyametdinov, Y.; Kusz, J.; Gütlich, P. *J. Am. Chem. Soc.* **2008**, *130*, 1431. (b) Gaspar, A. B.; Seredyuka, M.; Gütlich, P. *Coord. Chem. Rev.* **2009**, *253*, 2399.
(5) Muñoza, M. C; Real, J. A. *Coord. Chem. Rev.* **2011**, DOI: 10.1016/j.ccr.2011.02.004.
(6) (a) Clemente-León, M.; Coronado, E.; López-Jordà, M.; Mínguez-Espallargas, G.; Soriano-Portillo, A.; Waerenborgh, J. C. *Chem.—Eur. J.* **2010**, *16*, 2207. (b) Clemente-León, M.; Coronado, E.; López-Jordà, M.; Desplanches, C.; Asthana, S.; Wang, H.; Létard, J.-F. *Chem. Sci.* **2011**, *2*, 1121.
(7) Nihei, M.; Takahashi, N.; Nishikawa, H.; Oshio, H. *Dalton Trans.* **2011**, *40*, 2154.
(8) Cheng, H.; Djukic, B.; Jenkins, H. A.; Gorelsky, S. I.; Lemaire, M. T. *Can. J. Chem.* **2010**, *88*, 954.
(9) (a) Barth, P.; Schmauss, G.; Specker, H. *Z. Naturforsch.* **1972**, *27B*, 1149. (b) König, E.; Ritter, G.; Schnakig, R. *Chem. Phys. Lett.* **1974**, *27*, 23.
(10) (a) Yu, Z.; Li, C.; You, X. Z.; Spiering, H.; Gütlich, P.; Hsia, Y. F. *Mater. Chem. Phys.* **1997**, *48*, 150. (b) Ksenofontov, V.; Levchenko, G.; Spiering, H.; Gütlich, P.; Létard, J.-F.; Bouhedja, Y.; Kahn, O. *Chem. Phys. Lett.* **1998**, *294*, 545.
(11) (a) Wei, H.-H.; Kao, S.-P.; Jean, Y.-C. *Trans. Met. Chem.* **1986**, *11*, 405. (b) Oso, Y.; Ishida, T. *Chem. Lett.* **2009**, *38*, 604.
(12) (a) Létard, J.-F.; Guionneau, P.; Codjovi, E.; Lavastre, O.; Bravic, G.; Chasseau, D.; Kahn, O. *J. Am. Chem. Soc.* **1997**, *119*, 10861.
(13) Otwinowski, Z.; Minor, W. *Methods in Enzymology, Macromolecular Crystallography, Part A*; Carter, C. W., Sweet, R. M., Eds.; Academic Press: London, 1997; Vol. 276, pp 307−326.
(14) Blessing, R. H. *Acta Crystallogr.* **1995**, *A51*, 33–38.
(15) Sheldrick, G. M. *Acta Crystallogr.* **2008**, *A64*, 112–122.
(16) Schafer, A.; Huber, C.; Ahlrichs, R. *J. Chem. Phys.* **1994**, *100*, 5829–5835.
(17) (a) Godbout, N.; Salahub, D. R.; Andzelm, J.; Wimmer, E. *Can. J. Chem.* **1992**, *70*, 560–571. (b) Reed, A. E.; Curtiss, L. A.; Weinhold, F. *Chem. Rev.* **1988**, *88*, 899–926.
(18) Gorelsky, S. I. *AOMix*, version 6.46 ed.; University of Ottawa: Ottawa, Canada, 2010.
(19) Gorelsky, S. I.; Lever, A. B. P. *J. Organomet. Chem.* **2001**, *635*, 187–196.
(20) (a) Sur, S. K. *J. Magn. Reson.* **1989**, *82*, 169–173. (b) Evans, D. F. *J. Chem. Soc.* **1959**, 2003–2005. (c) Chambers, J.; Eaves, B.; Parker, D.; Claxton, R.; Ray, P. S.; Slattery, S. J. *Inorg. Chim. Acta* **2006**, *359*, 2400–2406.
(21) (a) Paulsen, H.; Trautwein, A. X. *Top. Curr. Chem.* **2004**, *235*, 197. (b) Shiota, Y.; Sato, D.; Juhász, G.; Yoshizawa, K. *J. Phys. Chem. A* **2010**, *114*, 5862. (c) Ye, S.; Neese, F. *Inorg. Chem.* **2010**, *49*, 772.